Journal of Hydrology 529 (2015) 316–329

Contents lists available at ScienceDirect

Journal of Hydrology

journal homepage: www.elsevier.com/locate/jhydrol

Field test of a multi-frequency electromagnetic induction sensor for soil moisture monitoring in southern Italy test sites

G. Calamita [a,*], A. Perrone [a], L. Brocca [b], B. Onorati [c], S. Manfreda [d]

[a] Institute of Methodologies for Environmental Analysis (IMAA), National Research Council, Tito Scalo, Italy
[b] Research Institute for Geo-Hydrological Protection (IRPI), National Research Council, Perugia, Italy
[c] School of Engineering, University of Basilicata, Potenza, Italy
[d] Department of European and Mediterranean Cultures, University of Basilicata, Matera, Italy

ARTICLE INFO

Article history:
Received 18 April 2015
Received in revised form 10 July 2015
Accepted 17 July 2015
Available online 22 July 2015

This manuscript was handled by Corrado Corradini, Editor-in-Chief, with the assistance of Juan V. Giraldez, Associate Editor

Keywords:
Electromagnetic induction
GEM-300
Soil moisture
Field survey
Hillslope scale
Fiumarella di Corleto

SUMMARY

Soil moisture is a variable of paramount importance for a number of natural processes and requires the capacity to be routinely measured at different spatial and temporal scales (e.g., hillslope and/or small catchment scale). The electromagnetic induction (EMI) method is one of the geophysical techniques potentially useful in this regard. Indeed, it does not require contact with the ground, it allows a relatively fast survey of hillslope, it gives information related to soil depth greater than few centimetres and it can also be used in wooded areas. In this study, apparent electrical conductivity (EC_a) and soil moisture (SM) measurements were jointly carried out by using a multi-frequency EMI sensor (GEM-300) and Time Domain Reflectometry (TDR) probes, respectively. The aim was to retrieve SM variations at the hillslope scale over four sites, characterized by different land-soil units, located in a small mountainous catchment in southern Italy. Repeated measurements of EC_a carried out over a fixed point showed that the signal variability of the GEM-300 sensor (Std. Err. ~[0.02–0.1 mS/m]) was negligible. The correlation estimated between point EC_a and SM, measured with both portable and buried TDR probes, varied between 0.24 and 0.58, depending on the site considered. In order to reduce the effect of small-scale variability, a spatial smoothing filter was applied which allowed the estimation of linear relationships with higher coefficient of correlation ($r \sim 0.46$–0.8). The accuracy obtained in the estimation of the temporal trend of the soil moisture spatial averages was in the range ~4.5–7.8% v/v and up to the ~70% of the point soil moisture variance was explained by the EC_a signal. The obtained results highlighted the potential of EMI to provide, in a short time, sufficiently accurate estimate of soil moisture over large areas that are highly needed for hydrological and remote sensing applications.

1. Introduction

Soil moisture (SM) plays a crucial role in a large number of natural processes acting at different scales either in space or in time. It is involved in both the water and the energy cycles and influences hydrogeological (Brocca et al., 2012a, 2012b; Bronstert et al., 2012; Penna et al., 2011; Manfreda and Fiorentino, 2008), eco-hydrological (Manfreda and Caylor, 2013; Rubol et al., 2013) and climatic processes (Seneviratne et al., 2010).

SM can be measured in different ways by using *in-situ* or remote sensing (RS) methods. Being invasive, time-consuming, labour intensive and destructive, the standard thermo-gravimetric method has been progressively and extensively substituted by the use of indirect methods (Robinson et al., 2008a). Among these, thanks to the high accuracy and time resolution attainable, the most widely used are those based on the Neutron thermalization (Evett et al., 2008), i.e. Neutron Moisture Meters (NMM), and on the measurement of the dielectric properties of the soil, i.e. time-domain reflectometry (TDR), capacitance and time-domain transmission (TDT) sensors (Vereecken et al., 2014). These methods reveal limitations that have been only partially solved with the introduction of distributed sensor networks for the estimation of SM at the field, slope and small catchment scale.

In this regards, methods based on Cosmic-Ray Neutrons and Global Positioning System (GPS) signals have received attention. Indeed, both methods allow the accurate retrieval of a field-averaged SM with a temporal resolution that is of interest for hydrological applications. The cosmic-ray method is based on the measurement at the soil surface of cosmic-ray neutrons

* Corresponding author.
E-mail address: giuseppe.calamita@imaa.cnr.it (G. Calamita).

http://dx.doi.org/10.1016/j.jhydrol.2015.07.023
0022-1694/

generated by the soil and attenuated by hydrogen atoms (Vereecken et al., 2014; Zreda et al., 2012). The disturbance due to the presence of other hydrogen sources near the Earth's surface (i.e. water vapour, vegetation water, soil organic matter, etc.) within the sensing distance of the probe (Ochsner et al., 2013) is the main limitation of the method. GPS signals (Microwave L-band) travelling between GPS satellite and receiving antenna gather, in addition to the direct signal, the energy reflected from the ground. The elevation angle of the reflections, the dielectric properties and the roughness of the soil are the main controls of the reflected GPS signal (Larson et al., 2008). This method provides measurements at the skin surface (~5 cm) and is also limited by the presence of vegetation covers and by its static nature.

Whereas in the past attention was devoted to high measurement accuracy and precision over few points, an improved understanding of the processes and factors that control SM patterns might derive from measurements that sense greater soil volumes, taken in a larger number of points, distributed over larger scales, albeit with lower accuracy (Tromp-van Meerveld and McDonnell, 2009; Robinson et al., 2008a, 2008b). This would smooth out less important details, deriving from multi-point measurements, and would emphasize the emerging features at larger scales (McDonnell et al., 2007; Sivapalan, 2003). Geophysical methods have the potential to go beyond the local information sensed with traditional sensors (thermo-gravimetric, NMM, TDR, etc.) and to help filling the gap between the hillslope space–time scales of interest and the established methods available for SM measurement (see Fig. 3 in Robinson et al., 2008b). Promising results for soil-hydrologic studies have already been showed by methods such as Ground Penetrating Radar (Huisman et al., 2002), Electrical Resistivity (Calamita et al., 2012; Samouëlian et al., 2005) and Electro-magnetic Induction (EMI) (Vereecken et al., 2014). In particular, a renewed interest has emerged towards the EMI method for small catchment studies (Robinson et al., 2012). Indeed, ground-based EMI sensors are lightweight and do not require contact with the soil allowing a considerable reduction of the survey duration. Moreover, the ability of measuring through thicknesses of soil greater than few centimetres and the possibility to collect data in wooded areas makes the use of ground-based EMI sensors of high interest. The technological development and the introduction of multi-frequency sensors can further promote the use of this method allowing to quickly obtaining information at different depths of investigation (Doolittle and Brevik, 2014).

The soil property measured by EMI sensors is a complicated average of local electrical conductivities distributed in the volume of soil sensed that is a function of the physical properties of the soil, i.e. pore water electrical conductivity (EC_w), SM, mineralogical composition, soil texture and temperature (Callegary et al., 2007; Friedman, 2005). Additional sources of noise can be natural and anthropic, i.e. powerlines, broadcasting airwaves, buried cables/pipelines, air electricity caused by near or distant thunderstorms with lightning discharges (sferic events) (Huang, 2005). The simultaneous interplay of a number of environmental variables on the sensor response is a common downside with other methods such as RS active microwave techniques for which the sensor response is influenced not only by the dielectric constant of the soil but also by superficial roughness, soil texture, vegetation density and by temperature (Robinson et al., 2012).

EMI sensors have been largely tested for a quite large number of environmental issues (Doolittle and Brevik, 2014) such as: the detection of buried utilities and services (El-Qady et al., 2014), the detection and tracing of archaeological remains (De Smedt et al., 2013), the imaging of permafrost (Dafflon et al., 2013), the depth-to-clay estimation (Saey et al., 2009), the definition of groundwater levels (Sherlock and McDonnell, 2003; Buchanan and Triantafilis, 2009), the assessment of soil pollution and soil quality (Corwin and Lesch, 2005), the spatial pattern delineation of the soil textures (Abdu et al., 2008) and plant communities (Robinson et al., 2008c), the interpretation of hydrological/biogeochemical processes (Robinson et al., 2009) and the determination of the spatial variability of soil salinity (Doolittle et al., 2001) represent some of the most common applications.

A number of papers published in the last three decades in different fields, such as precision agriculture, soil and vegetation science, water resource management, has somehow tackled the use of EMI sensors for the determination of the spatial or temporal patterns of SM. Table 1 provides a synoptic view of the most relevant papers published in this research area. Columns summarize the main features of the studies such as location, sensors, soil texture/type, land cover, spatial and temporal scales, sampling scheme etc.

As already highlighted by Tromp-van Meerveld and McDonnell (2009), the majority of the published papers were carried out using a mono-frequency EMI sensor (EM31, EM38 and Dualem-1S) in agricultural fields (Hanson and Kaita, 1997; Akbar et al., 2005; Hezarjaribi and Sourell, 2007; Huth and Poulton, 2007; Robinson et al., 2009; Hossain et al., 2010; Padhi and Misra, 2011; Hedley et al., 2013) or in sites with no- or limited vegetation (Sheets and Hendrickx, 1995; Khakural et al., 1998; Scanlon et al., 1999; Sherlock and McDonnell, 2003; Brevik et al., 2006; Popp et al., 2012). To date, the number of studies conducted in forested highlands is very limited (Robinson et al., 2008c; Tromp-van Meerveld and McDonnell, 2009).

Except few cases (Hezarjaribi and Sourell, 2007; Kachanoski et al., 1988; Padhi and Misra, 2011) and irrespective of the soil texture, a simple linear function proved to satisfactory describe the relation between SM and EC_a measurements (Table 1). The analysis of the published papers also shows that the spatial and temporal variance of SM explained by EMI-EC_a data is highly varying. Fig. 1 provides a summary of the reported R^2 of the linear fit in the reviewed papers. Since the solid particle properties and pore water conductivity (EC_w) can be considered almost unchanging in time, SM variations represent the major factor influencing the EC_a of soils with a low content of 2:1 clays. This may explain why generally, higher correlations are showed in temporal domain (blue colour) compared to the spatial domain (red colour). Sheets and Hendrickx (1995) acquired, in an arid region, monthly EC_a data and SM (in the top 1.5 m) along a ~2 km transect for 1.5 year. They estimated that up to 64% of SM temporal variability and up to 46% of the SM spatial variability were explained by EM31-EC_a. Sherlock and McDonnell (2003), during one single survey, found that up to 70% of (gravimetrically determined) SM in the first 0.2 m of a $50 \times 50\ m^2$ pastureland hillslope was described by EM38-EC_a. Robinson et al. (2008c) found that Dualem-1S EC_a, spatially smoothed by kriging, explained 73% of the observed SM in the top 0.3 cm on one measurement date in a 41 ha mountainous basin. Robinson et al. (2012) carried out a study on a 4 ha mixed Oak – grass savanna catchment. Interpolated maps of TDR-SM in the top 0.15 m and EMI-SM showed a $R^2 = 0.28$.

To our knowledge, only Tromp-van Meerveld and McDonnell (2009) tested a multi-frequency EMI sensor (GEM-300) to monitor SM. For a nine months experiment over an upland forested hillslope ($\sim 8.8 \times 10^2\ m^2$), where quite dense sampling was carried out (2–4 m sampling step), the four frequencies used, in the range ~[7–14 kHz], resulted to be highly correlated to each other. The relation in the time domain between the hillslope average EC_a and hillslope average SM was only slightly better at depths ~>0.3 m ($R^2 \sim 0.84$–0.87) than at depths ~ <0.15 m ($R^2 \sim 0.78$–0.83). A limitation of this work concerns the chance to compare EC_a and SM values with other published papers. Indeed, they reported an EC_a range of ~[−30, +30 mS/m] that might be due to a calibration protocol of the GEM-300 sensor not explained in the text. Also, SM values are expressed as Aqua-pro values, ranging

Table 1
Main characteristics of the previous studies on the application of the EMI method for SM estimation (TG: Thermo-gravimetric method; TM: Tensiometer; PP: Pressure Plate; TP: Theta Probe; AP: Aqua-pro capacitance sensor; *N*: sample size, R^2: coefficient of determination).

Reference	Location	Soil texture	Soil type/soil definition	Land cover	Spatial scale (mq)[a]	Spacing (m)	Scheme	Temporal scale (d)[b]	Temporal sapling[c]	*N*[d]	SM probe	EMI sensor	R^2[b]	Type of relation	SM depth (m)
Kachanoski et al. (1988)	Canada	5–70% sand 26–64% silt 2.5–44% clay	Luvisolic		1.50E+04	10–15	Transects	1		52	TDR	EM31 EM38	0.77–0.88 0.96	Linear Second order poly	0.5
Kachanoski et al. (1990)	Canada	Moderately fine textured calcareous	Chernozemic		6.60E+02	10	Transect	90[e]	3 SM, 1 EC_a	66	NMM	EM31 EM38	0.38–0.67	Linear	1.7
Sheets and Hendrickx (1995)	USA	72.5% sand 14% clay	Fine and coarse loamy		1.95E+03	30	Transect	480	16	65 1040	NMM	EM31	0.11–0.46 0.58–0.64	Linear	1.3
Hanson and Kaita (1997)	USA	30% sand 52% silt 18%clay	Clay loam	Sorghum field	9.00E+00[f]		Point	35	15[g]		NMM	EM38	0.76–0.95	Linear	1.2
Khakural et al. (1998)	USA	33% sand 40% silt 27%clay	Fine loam – Silty clay loam		1.68E+04	10–15[g]	Transects[h]	1		14	NMM	EM38	0.5–0.8	Linear	1
Scanlon et al. (1999)	USA	Clay (Playa site)		Mesquite trees-Tobosagras – Herbs	8.00E+02	10	Transect/ Borehole	480	5–6	7–20	TG	EM31 EM39	0.11–0.85	Linear	6
Reedy and Scanlon (2003)	USA		Sandy clay loam	Engineered cover	5.78E+02	3–28.5	Irregular grid	1095	36	10	NMM	EM38	0.80–0.84	Linear	1.5
Sherlock and McDonnell (2003)	USA		Coarse loam	Pastureland	2.50E+03	5	Grid[h]	1		33	TG	EM38	0.6–0.7	Linear	0.2
										19	TM		0.01–0.15		
Akbar et al. (2005)[i]	USA	10.4% sand 33.5% silt 56.2% clay	Fine clay (Vertisol)	Corn field	9.00E+04		Irregular grid	270	2	11	TG	EM38	0.13–0.43	Linear	1.2
		28.3% sand 46.1% silt 21.4% clay	Silty clay loam	Cotton field	1.60E+05			180		25			0.13–0.50		
Brevik et al. (2006)	USA		Fine loam (Mollisol)	Grass	9.00E+01	25–30	Transect	120[j]	13–14	100	TG	EM38	0.5–0.90	Linear	0.9
Hezarjaribi and Sourell (2007)	Germany		Loamy sand – Sand	Agricultural field	8.20E+04	2–3 × 4–6[k]	Dense grid[h]	1		29	TG- PP	EM38	0.35–0.56	Second order	0.6
Huth and Poulton (2007)	Australia		Clay vertosol	Field with wheat, cotton, chickpeas and Eucalyptus	5.00E+01	2–6	Transect	300	4			EM38	0.93	Linear	0.9
Robinson et al. (2008c)	USA	38.4% silt 19.2% clay – 47.7% silt 22.3% clay	Gravelly loam Gravelly silt loam	Shrub-grass Woody	4.10E+05	Irregular[k]	Irregular[h]	1[l]		40	TG	Dualem-1S	0.73		0.3
Robinson et al. (2009)	Cambodia		Deltaic sediment	Agriculture during dry season	4.00E+00 2.72E+04[g]	Irregular[k]	Point Irregular	21 1		9	TP TG	Dualem-1S	0.91 0.24	Linear Linear	0.4 0.6
Tromp-van Meerveld and McDonnell (2009)	USA		Sandy loam	Forested	8.80E+02	2–4	Irregular grid	270	57[m]	64	AP	GEM-300	0.1–0.99	Linear	1.8
Hossain et al. (2010)	Australia		Black Vertosol		1.00E+04	Irregular	Irregular	1		17	TGc	EM38	0.37–0.56	Linear	1.2
Padhi and Misra (2011)	Australia	10% sand 14% silt 76% clay	Clay soil (Black Vertosol)	Wheat field	3.12E+03	20	Point	145	12	12	NMM	EM38	0.7–0.8	Linear – exponential	1.33
Popp et al. (2012)	Austria	Calcite < 40% quartz 25–40% clay < 30%	Loamy scree, glacial till	Meadow	1.30E+05	Irregular	Irregular	1		18	TG	EM38	0.16–0.39	Linear	0.4

Table 1 (*continued*)

Reference	Location	Soil texture	Soil type/soil definition	Land cover	Spatial scale (mq)[a]	Spacing (m)	Scheme	Temporal scale (d)[b]	Temporal sapling[c]	N^d	SM probe	EMI sensor	R^b	Type of relation	SM depth (m)
Hedley et al. (2013)	New Zealand	90–96% sand 2–4% clay	Motuiti sand	Maize field	7.5E+05	10 × 4[k]	Transect[h]	30	1[n]	9	Delta-T SM300 (Sensor network)	EM38	0.77–0.94[o]	Multiple Linear Regression Random Forest	0.5
Robinson et al. (2012)	USA		Clay-silty clays-sandy loams–loams	Oak-grass savanna	4.00E+04	Irregular[k]	Irregular	180	1 SM, 6 ECa	Interpolated values	TDR	Dualem-1S	0.28–0.48[1o]	Linear	0.15

[a] When a transect scheme was used, the area extent was calculated multiplying the transect length times 1 m. When replicates are present the scale is that reported in the result section.
[b] Approximate number of days [d]: a month is roughly approximated to 30 days, one year to 365 days.
[c] Number of surveys.
[d] Number of points where both SM and EC_a are measured during a single survey.
[e] SM and EC_a data collected during different days.
[f] Three replicates of a 3 × 3 m^2 field.
[g] Deduced from paper figures.
[h] Irregular SM sampling.
[i] Correlations estimated from table data.
[j] For each of two consecutive years.
[k] Then interpolated.
[l] Two days were necessary to cover the entire study area.
[m] More dense in winter and early spring.
[n] One ECa survey; SM data aggregated from measurement made each 15 min.
[o] Correlation between SM measured by means of TDR probes and SM estimated by means of EC_a data.

between 0% and 100%, without explicitly mention the calibration parameters for the conversion.

The current study aims at adding a piece of knowledge in the understanding of the potential of the multi-frequency GEM-300 for shallow SM retrieval during a whole hydrological year at the hillslope scale for sites located in a mountainous and forested small catchment belonging to the Agri Basin in southern Italy (Basilicata region). Specific objectives of the work are: (i) the comprehension of issues related to the inherent precision of the GEM-300 sensor that, to our knowledge, were never addressed before; (ii) the comparison of frequencies in the range ~[7–20 kHz] for the retrieval of shallow SM; (iii) the assessment of the suitability of the EMI-EC_a response to represent SM variations for larger hillslopes, characterized by different soil type, morphology, lithologic parent material and land cover.

2. Site description

The experimental river basin "Fiumarella di Corleto" is located in the Basilicata region in southern Italy. It has an extent of about 32.5 km^2 with the elevation ranging between ~630 and 1380 m above sea level (Fig. 2). The mean annual precipitation is ~720 mm and the mean annual temperature is ~9.9 °C. The climate zone of the basin is classified as sub-humid. The hydrology of the basin is continuously monitored through three permanent weather stations (Manfreda et al., 2011).

The basin is characterized by two opposite slopes (north-eastern and south-western) that clearly show different geological and morphological features in terms of soil-landscape units: the north-eastern slope is mostly covered by forests, whereas the south-western one is mostly exploited for agricultural purposes. Additional information about land cover features and hydraulic properties characteristics of the soils in the Fiumarella catchment are available elsewhere (Santini et al., 1999; Romano and Palladino, 2002; Fiorentino et al., 2006; Carriero et al., 2007).

The sites of measurement were chosen with the aim to select the most representative land-soil units characterizing the basin (Fig. 2 and Table 2). Table 2 sums-up the main characteristics of the mentioned sites and of the number of surveys carried out on each of them. Very recently Cavalcante et al. (2015) characterised the mineralogical composition of the clayey content in different zones of the catchment highlighting the widespread presence of illite–smectite mixed clay layers. Moving from the central and western part of the catchment through the northern up to the southeast, they observed progressively higher proportions of smectite compared to illite. The minerals of the smectite groups are basically 2:1 clays characterized by a high value of cation exchange capacity (CEC).

3. Methods and materials

The frequency-domain EMI sensors generate an oscillating electromagnetic (EM) field ('primary'), which propagates in the soil. The primary field induces alternating currents, which, in turns, produce another EM field ('secondary') measured by the sensor. Under conditions known as 'low induction number' (LIN) a linear relationship exist between the quadrature component of the secondary EM field and the EC_a of the volume of soil through which the EM field propagates (Callegary et al., 2007, 2012; Sharma, 1997).

In the "Fiumarella di Corleto" catchment EC_a measurements were made using the GEM-300 (Geophysical Survey Systems Inc., North Salem, NH), a portable, digital, multi-frequency EMI sensor that can operate in the frequency range 300–20,000 Hz. The GEM-300 is equipped with a transmitting coil (Tx), a receiving coil

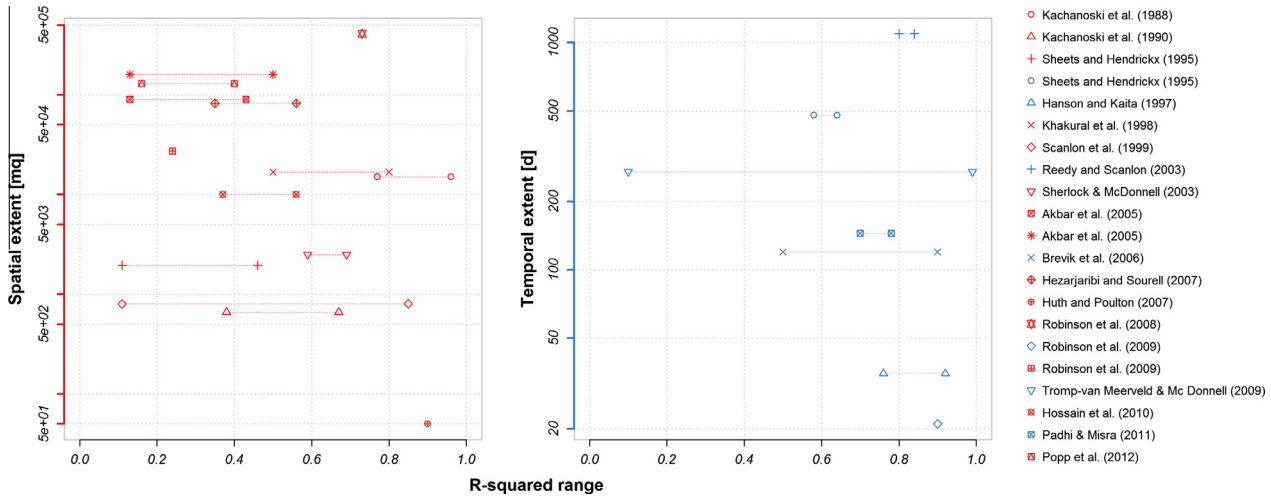

Fig. 1. SM variance explained by EMI-EC_a measurements according to the reviewed literature. The red colour is used for spatial variations (left) and the blue colour for the temporal ones (right). (For interpretation of the references to colour in this figure legend, the reader is referred to the web version of this article.)

(Rx), and a third coil, named "bucking", used to remove the primary field influence at the Rx. The distance, *s*, between Tx and Rx is fixed at 1.6 m.

3.1. Depth of investigation

The penetration depth of the GEM-300 sensor is assumed to be limited by the "skin depth" (δ) (Won et al., 1996; Doolittle et al., 2001). This physical quantity is the depth at which the amplitude of an EM wave is attenuated by a factor equal to e^{-1} of the original amplitude. For a fixed coil separation, *s*, the skin depth decreases with the increase of the square root of both the frequency used for the sounding and the EC of the conductor (Sharma, 1997). The actual thickness of soil influencing the measurement, named depth of investigation, DOI, (also known as depth of exploration or depth of observation) is an empirical concept that is difficult to estimate accurately. In fact, DOI is influenced by several factors, i.e. sensor sensitivity, operating frequencies, coil configuration, soil EC contrasts, ambient noise level (power/phone lines, fences, sferics), etc. (Huang, 2005). The actual DOI is some orders of magnitude smaller than the skin depth, as indicated by physical (Spies, 1989; Huang, 2005) and numerical (Callegary et al., 2007, 2012) studies.

In this work, six frequencies in the range of ~7200–20,000 Hz were used. This range contains the frequencies of the most used mono-frequency EMI sensors, i.e. EM31 (9800 Hz), EM38 (14,600 Hz) and DUALEM-1S (9000 Hz) and the frequencies used in the paper of Tromp-van Meerveld and McDonnell (2009), i.e. 7275, 9075, 11,275 and 14,025 Hz. In addition, two higher frequencies, i.e. 16,325 and 19,950 Hz, were chosen due to their theoretical shallower DOI. Following Huang (2005), a rough estimation of the DOI for these frequencies would be of ~<6.5 m for soils with EC_a of 20 mS/m, whereas for soils with EC_a ranging up to 160 mS/m the DOI would be attenuated to ~<3.8 m. Callegary et al. (2007) showed that for soils with such conductivities the DOI is reduced between ~1.1*s* and ~0.5*s*, which corresponds to ~1.8 and ~0.8 m depth. However, since a vertical sensitivity curve for the GEM-300 has not been fully explored in the literature, for the frequencies used there is an evidence that the sensitivity of sensor response is higher for shallower soil layers (Doolittle et al., 2001; Tromp-van Meerveld and McDonnell, 2009).

3.2. Temperature correction

Temperature is known to influence EC_a measured with EMI sensors in two way (i) by causing a thermal drift and (ii) by acting on the mobility of dissolved ions in the soil pore water. Unfortunately, no relevant published papers focusing on the effect of thermal drift for the GEM-300 sensor are available in literature. Sudduth et al. (2001) carried out stability tests on the EM38 sensor (Geonics Ltd) finding contrasting results between measurements repeated in time over a fixed point and over a transect. Authors concluded that the thermal drift in the measurements could be not a function of air temperature but rather it could be caused by the instability of the instrument. Tromp-van Meerveld and McDonnell (2009) claimed a non-linear relationship between the air temperature and EC_a (data not shown).

Among the various models proposed for the correction of the temperature effect on the mobility of dissolved ions, the "corrected Sheets and Hendrickx model", which is the best performing in most of the situations and for a wide range of temperature according to Ma et al. (2011), was adopted here:

$$EC_{25} = EC_a(0.447 + 1.4034e^{-T/26.815}), \quad (1)$$

where the EC_{25} represents the EC_a value at the reference temperature of 25 °C. Since soil temperature data were not available for the temperature correction of the EC_a, the mean daily air temperature of the week prior to the surveys were used as a proxy. The first site (A) was surveyed always around 9–10 AM, while the last site (D) after about 3–4 h. During each field survey, the air temperature was increasing, but due to the lack of hourly temperature data, such fluctuation was neglected. At the beginning of the day and before starting the measurements, the GEM-300 sensor was left outside for 20–60 min. This time was necessary to give the sensor the time to reach a thermal equilibrium thus avoiding potential thermal drift effects. Considering that the time required to survey each site with the EMI was 15 min, it was assumed no change in the air/soil temperature.

3.3. Field data acquisition

During each survey, SM and EC_a were measured at 25 points placed at a distance of 20 m on a 80 × 80 m^2 grid. The only exception was represented by the site C, where the constraints posed by

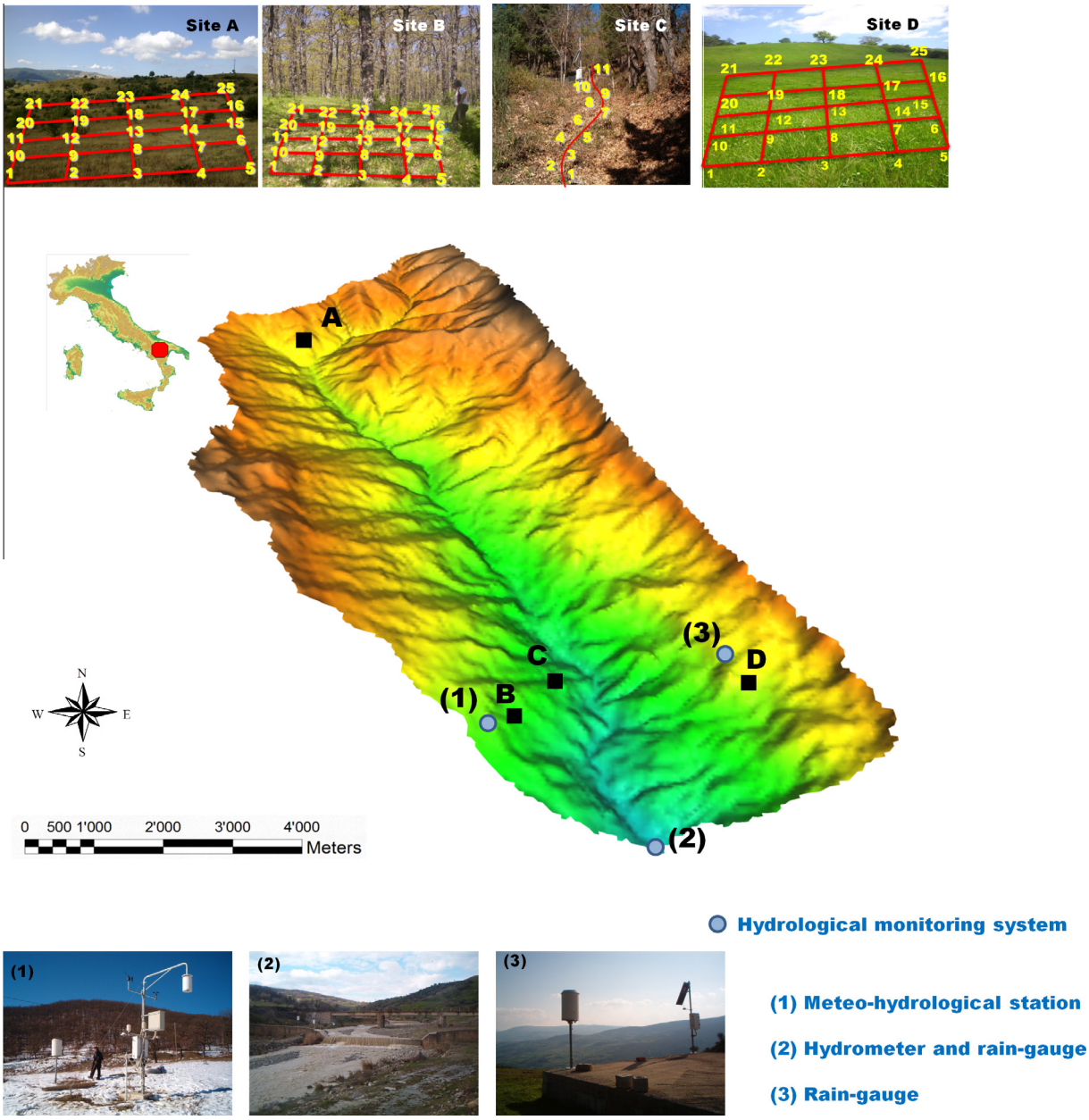

Fig. 2. General description of the experimental basin "Fiumarella di Corleto", Basilicata region (southern Italy). Geographical location of the basin and its experimental setup.

Table 2
Summary of the relevant characteristics and number of the surveys carried out for each surveyed field (#P, number of points; #S, number of surveys).

Acronym	Site name	Land use	Soil texture	Sampling scheme	Lithology	Spacing (m)	#P	#S	Slope
Site A	Monte Caperrino	Shrubs and grass	Silty-loam	Regular grid	Gorgoglione Formation Pelitic Arillaceous lithofacies	20	25	8	3–5%
Site B	Masseria Falcone	Sparse wood	Silty-clay	Regular grid	Argille Varicolori Formation	20	25	4	2–3%
Site C	Transect	Natural dense wood	Clay-loam	Transect	Argille Varicolori Formation	5.5	11	10	15–18%
Site D	Masseria Potenza	Agricultural	Silty-loam	Regular grid	Torrente Cerreto Unit	20	25	7	15–18%

the dense vegetation and the local morphology forced the use of a transect of 60 m length with 11 sampling points (Fig. 2). To ensure repeatability and avoid interference with the EMI sensor, small wooden stakes were used to indicate the grid nodes. In order to maximize the range of SM values sampled, surveys were carried out during different periods of a whole hydrological year, from May 2012 to May 2013. Typically, the time necessary for the EMI measurements was 3–4 times less than that required for SM. During the entire study period 695 point measurements of both EC_a and SM were acquired. Logistic constraints (i.e., unexpected instrumental failures, rainstorms, excessive hardness of the terrain) limited the number of sites monitored during few field surveys.

At sites A, B and D, measurements of SM in the first 15 cm were made using a portable two-wire connector-type Time Domain Reflectometer (TDR) MiniTrase 6050X3 (Soil Moisture Equipment

Corp., 1996). At site C, SM was measured hourly by 22 buried TDR sensors (TDR100, Campbell Scientific) placed at eleven points along the transect to the depth of 0.3 and 0.6 m. The volumetric SM values (% cm^3/cm^3) were estimated through the calibration equation of Topp et al. (1980) using the estimates of the dielectric constant furnished by the TDR sensor.

EC_a measurements were always made following the same path of points and were always collected by the same operator in order to minimize the sensor variability due to height from ground, orientation and tilt. The most practical vertical dipole configuration with sensor held at hip height was chosen. In order to reduce the influence on the EMI sensor, measurements at site C were made at >1 m away from the buried TDR probes, whenever possible (Stanley et al., 2014). However, in this site a number of potential interfering metallic features were also present (iron pegs, fence with wire mesh).

The instrumental (random) error of the GEM-300 in the field has been assessed under different environmental conditions (i.e. temperature, SM states, etc.). A single point located in the wood at ~100 m apart from site C transect was used to carry out repeated EC_a measurements for six different days. A variable number of measurements (Fig. 3) was acquired holding the sensor at the same (hip) height and orientation. The tests lasted a few minutes (~1–3) during which changes in the air temperature were neglected.

3.4. Data analysis

The quality of both SM and EC_a data was preliminarily checked. The buried TDR probes installed along a transect at the site C can occasionally fail to acquire data or return SM values not physically meaningful, because greater than the known soil porosity or lower than the residual SM. To fix this issue, the hourly SM time series have been filtered removing all values exciding the local maximum assumed equal to the soil porosity. Thereafter, temporal gaps were reconstructed by using an interpolating function based on the use of splines. EC_a data were checked for consistency with surrounding data and with values registered at all the frequencies (1% of data was excluded).

Random variations of the repeated EC_a measurements over a single point were assessed by graphical analysis of the normal quantile–quantile plot (not shown) and the box and whiskers plot (boxplot). Compared to numerical tests, this graphical tool allows a comprehensive understanding of the degree and position of the deviations from normality. The instrumental precision was quantified using the standard error of the mean, defined as

$$\text{Std. Err.} = \sqrt{\frac{\sum_{i=1}^{N}(EC_{ai} - \overline{EC}_a)^2}{N-1}} \Big/ \sqrt{N} \quad (2)$$

where EC_{ai} represents the i-th observation, $\overline{EC}_a$ the mean value and N the number of observations.

In order to reduce abrupt changing in the space, both SM and EC_a gridded data were smoothed out by means of a moving average window. The filter was a 3×3 matrix centred on the point to be smoothed containing the weights of the neighbourhood. Weights were inversely proportional to distance and their sum was 1.

The precision of the calibration equation of the smoothed EC_a measurements for the estimation of the smoothed SM was assessed by means of the root mean square error (RMSE) as follow:

$$\text{RMSE} = \sqrt{\frac{\sum_{i=1}^{N}(SM_m - SM_f)^2}{N}} \quad (3)$$

where SM_m represents the measured SM, SM_f are the predicted values and N is the samples size of the calibration data set.

For the comparison of the predicted and the measured (smoothed) SM data both the RMSE and the mean absolute deviation, MAE, were used. The MAE is computed as the average deviation of the residual absolute values:

$$\text{MAE} = \frac{\sum_{i=1}^{N}\text{abs}|SM_m - SM_f|}{N} \quad (4)$$

The choice of the RMSE, as a measures of precision, and the MAE, as a measure for accuracy, has been made to simplify comparison with published works.

4. Results and discussions

4.1. GEM-300 sensor stability

Excluding the presence of occasional outliers, the graphical analysis of the data distributions revealed a reasonable symmetry in the data making plausible the assumption of approximate-normal distribution (Fig. 3a). The standard error varied in a narrow range between ~0.02–0.1 [mS/m] and did not show significant differences among frequencies (Fig. 3b). Moreover, standard error seemed to be not influenced by temperature and the EC_a mean value (Fig. 3b).

The mean EC_a values measured at 14.025 kHz were steadily lower of the values measured at other frequencies (of more than 5 mS/m). Considering the inverse relationships between frequency and DOI, it is possible to argue that the 14.025 kHz frequency might be more sensitive to an intermediate layer, which is less conductive than both over- and under-lying layers. This comparison makes it also plausible to think that the 14.025 kHz frequency may display a systematic shift towards lower conductivity values. Interestingly the range of values of EC_a observed in the six tests (14.025 kHz $\leqslant$ 11.275 kHz $\leqslant$ 9.075 kHz $\leqslant$ 7.275 kHz) is very similar to that reported by Tromp-van Meerveld and McDonnell (2009). Furthermore, it was noted that additional variability in the signal, which did not necessarily reflect a physical change in the subsoil, was due to sensor positioning (tilting, height) with respect to the ground as also showed by other authors (Stanley et al., 2014) for mono-frequency EMI sensors (i.e. EM38). In addition, Doolittle et al. (2001) comparing the EM38 and the GEM-300 pointed out an higher signal variability of the latter during in-field surveys.

4.2. Spatio-temporal variability of SM and EC_a

As regards to SM dynamics, a drying phase was observed from the beginning of May up to the end of October 2012 as clearly showed by site C data (Fig. 4a). Neglecting site B, where the drying-phase data are missing, it is possible to identify a distinct drying behaviour between dense vegetated (site C) and human-disturbed areas (site A and D). Indeed, the latter two sites exhibited more pronounced short term SM fluctuations during the drying period compared with the relatively smoother behaviour exhibited by SM in the wooded area, at both 30 and 60 cm of depth as pointed out recently by other authors (Manfreda et al., 2011). For instance, a quite intense rainfall event at the beginning of October 2012 (100 mm of rainfall in 6 days) caused an increase of surface SM values which clearly appears only at site A, probably due to the absence of vegetation interception and to the shallower soil depth at which SM was measured (15 cm vs 30/60 cm). At site D, as evidenced by the right tail of the distribution, there were few wet zones in the field whereas most of the field was still dry probably due to the ploughing operations that could have easily enhanced the loss of water from surface to deeper soil layers. Indeed, the

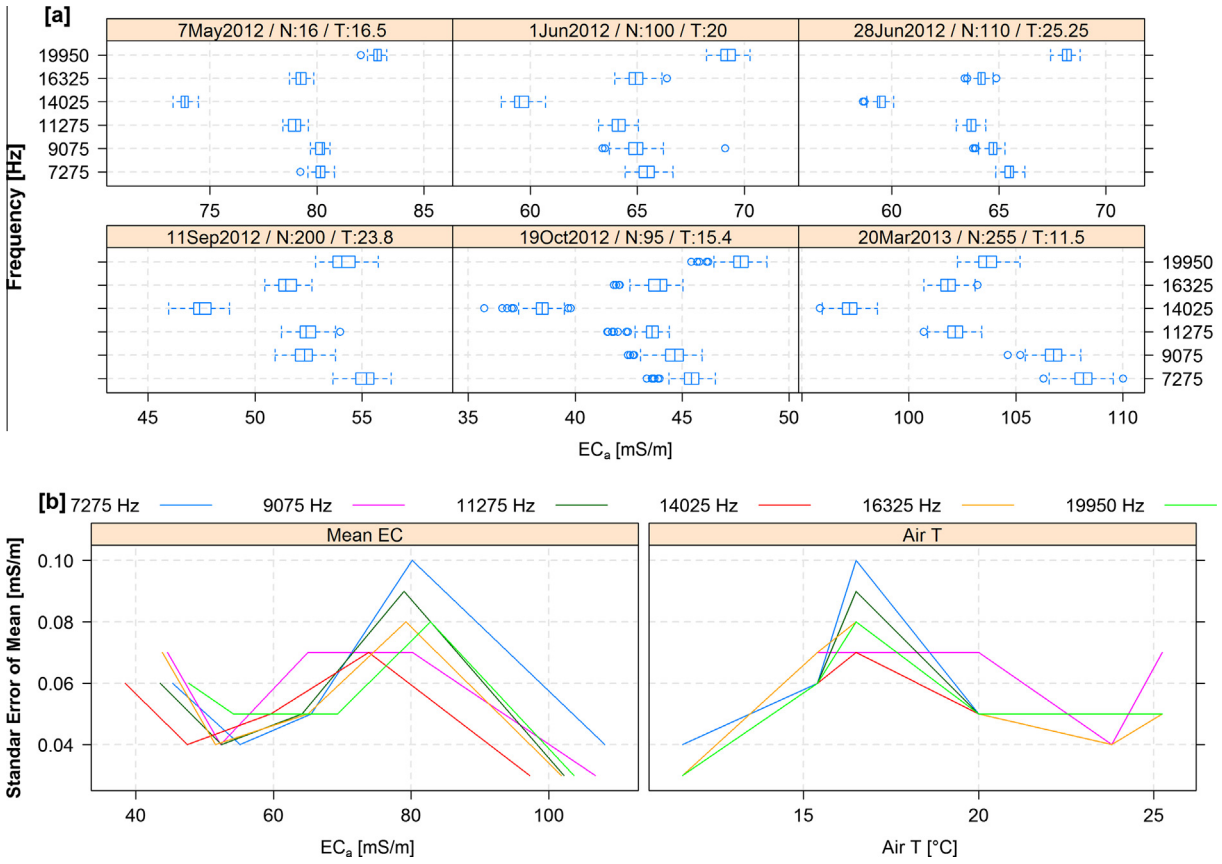

Fig. 3. (a) Distribution of the EMI measurements repeated over a fixed point for each frequency; the number of measurements (*N*) and the air temperature (*T*) are also reported. The bottom, the centre and the top of the boxplot represent, respectively, the first, the second and the third quartile of the data distribution. The whiskers extend 1.5 times the interquartile range (IQR). (b) The variation of the standard error of the mean EC_a for each frequency (colours) as a function of the measured EC_a value (right) and air temperature (left). (For interpretation of the references to colour in this figure legend, the reader is referred to the web version of this article.)

observed SM at site D was consistently lower than in other sites, especially at the end of the wetting phase. In contrast, SM measured in the forest covered areas (site C) rarely was lower than 20%. On average, the sites with the highest slope degree, i.e. site C and D, exhibited the highest values of SM spatial variability (Table 3) in accordance with previous studies (e.g., Brocca et al., 2009). Moreover, at site C (30 cm) the SM spatial variability decreased as the drying phase progressed, from May to October 2012, and went back to higher values after the wetting phase, occurred at the beginning of May 2013 (see Table 3 and Fig. 4a). Generally, SM showed a greater temporal than spatial variability especially in the A and D sites (see Table 3 and Fig. 4a).

The spatial variability was greater for EC_a than for SM, at every site (see Table 3 and Fig. 4b). This result is consistent with previous published studies (Calamita et al., 2012) and suggests that at the investigated sites factors other than SM contribute to the spatial variation of the EC_a. Also, at site C it is seen that the EC_a spatial variability decreased after the drying phase and increased after the wetting (Table 3) similarly to SM. However, at site C the temporal variability of EC_a exhibited larger values than that of SM (Fig. 4). On the contrary, at site A and D the SM varied in time much more than EC_a (Fig. 4). This was particularly evident for site D where the overlap of the standard error bars (Fig. 4b) indicate that a large uncertainty existed for the spatial EC_a mean, as also suggested by the higher spatial CV (Table 3). As could be expected by the small number of surveys and their proximity in time, at site B the smallest SM and EC_a spatio-temporal variation was observed.

4.3. Correlation analysis

An important issue to keep in mind when comparison between TDR-SM and EMI-EC_a are made concerns the different depths/volumes of investigation for the two methods applied. Whereas SM measurements refer to the top part of the soil (0.15 m) or to specific depth layers (0.3 and 0.6 m), the EC_a measurements sense a complex-shape volume of soil extending both laterally and to deeper soil layers (Callegary et al., 2012).

Whether the spatial or the temporal domain was considered, there were only slight differences in the relation between SM and EC_a for the six frequencies used. Generally, irrespective of the site and of the depth to which SM was measured, SM better correlated with the lowest frequency used, i.e. 7275 Hz (Fig. 5b). Data did not permit to verify the sensitivity of different frequencies respect to SM measurements made at 0.15 m and 0.3/0.6 m of depth. Indeed, EC_a values measured at different frequencies exhibited a very high degree of correlation between each other, slightly less than 1, confirming the results of previous studies (i.e. Doolittle et al., 2001; Tromp-van Meerveld and McDonnell, 2009). Doolittle et al. (2001) attributed to the high conductivity of the surface layer the close similarity of the EC_a spatial patterns measured with four frequencies, in the range ~[7–20 kHz]. Although no high conductive soil layer was present in their site, Tromp-van Meerveld and McDonnell (2009) could not resolve the SM depth profile. Moreover, they still noticed very similar responses for different frequencies even when SM displayed a non-uniform distribution with depth (i.e. after rain events). These results indicate that: (i) the 6 frequencies used in this study sense similar depths/volumes of

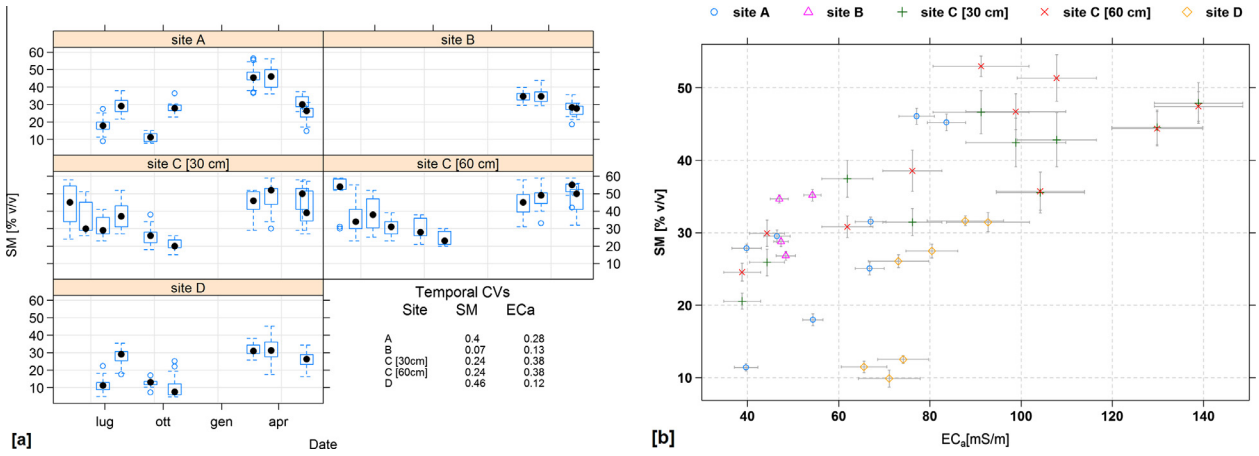

Fig. 4. (a) Temporal trends of SM spatial variability in each site during the study period, from May 2012 to May 2013. Boxplot legend as in Fig. 3. (b) Spatially aggregated SM and EC_a (7275 Hz) values and respective standard error bars.

soil; (ii) the sensor sensitivity is heavily influenced by the upper soil layers; (iii) shallow and deep SM are highly correlated. As regards to the last point, generally surface SM is not necessarily well correlated with the SM values integrated along the soil profile. In particular, a weak correlation is expected when topsoil is dry whereas the relation becomes stronger with the increase of surface SM values (see Manfreda et al., 2007). The lack of SM data at different soil depth and of a reference EMI sensor with a well documented depth-sensitivity response prevent from verifying these hypotheses. However, in view of the present result, the use of multi-frequencies appears to be of limited usefulness in studies of the dynamics of the vadose zone SM.

Following the above remarks, results related to only one frequency, i.e. 7.275 kHz, will be shown below. The correlation between point SM and EC_a values was overall higher for site C data (Fig. 5) where the depths of SM measurements (0.3–0.6 m) were more comparable with those of the GEM-300 and both SM and EC_a exhibited the highest spatial and temporal variability (see Table 3 and Fig. 4). As could be expected considering the different depth of investigations of the mobile TDR probes (0.15 m) and the GEM-300 sensor, a weaker relation between point SM and EC_a was found for the other sites (A, B and D). Among these sites, the highest correlation was found at site A whereas the lower were founded for site B and D ($r \sim 0.24$). The differences between sites A, B and D could be partially explained in terms of SM variability (see above). As already said, at site B the limited SM spatio-temporal variability prevented the estimation of a high correlation.

Although there was a high SM temporal variability at site D this was not adequately captured by that of EC_a. Indeed, during the dryer months (June–October) the soil was still relatively conductive (Figs. 4b and 5a). The poor SM-EC_a correlation at site D, could also been due to the physical soil properties and land use of the site. Indeed, the practice of soil chemical fertilization could have caused localized increase in the concentration of dissolved ions and, consequently, in the EC_w which might have contributed to the high spatial variability of the bulk EC_a (Corwin and Plant, 2005) and influenced the relation SM-EC_a (Hanson and Kaita, 1997). Moreover, the continuous remodeling of the soil by agricultural machines (compaction due to the wheels of tractors, plowing operations) could have substantially altered, in time and space, the structural attributes of the bulk soil solid-phase (e.g. soil density, porosity) that influence the EC_a measurements (Friedman, 2005). The high EC_a values during late-summer and early-autumn (Fig. 5) may be explained by a relatively higher presence of

Table 3
Spatial variability of SM and EC_a (7275 Hz) during each survey expressed as coefficient of variation (CV).

Date	SM					EC_a			
	Site A	Site B	Site C 30 cm	Site C 60 cm	Site D	Site A	Site B	Site C	Site D
2012-05-07	NA	NA	0.29	0.21	NA			0.27	
2012-06-01	NA	NA	0.26	0.24	NA			0.31	
2012-06-28	0.22	NA	0.2	0.24	0.34	0.19		0.29	0.38
2012-07-27	0.15	NA	0.22	0.16	0.17	0.32		0.3	0.37
2012-09-11	0.22	NA	0.24	0.2	0.22	0.31		0.31	0.41
2012-10-19	0.1	NA	0.18	0.16	0.6	0.45		0.4	0.49
2013-02-20	0.12	0.08	0.18	0.18	0.11	0.25	0.23	0.26	0.49
2013-03-20	0.13	0.11	0.19	0.14	0.22	0.24	0.19	0.25	0.51
2013-05-08	0.1	0.13	0.21	0.09	NA	0.25	0.17	0.38	
2013-05-15	0.18	0.11	0.26	0.18	0.17	0.23	0.22	0.39	0.48
Mean CV	0.15	0.11	0.22	0.18	0.26	0.28	0.20	0.32	0.45

smectite in the chaotic varicolored clay matrix rich of illite–smectite mixed layers as highlighted by Cavalcante et al. (2015). Smectite group minerals are 2:1 clays with a very high cation exchange capacity able to enhance the surface conduction mechanism in porous media (Binley et al., 2015).

The correlations between point EC_a and SM measured at similar depths are generally lower compared to other studies (e.g. Kachanoski et al., 1988; Sherlock and McDonnell, 2003). The fact that Kachanoski et al. (1988) averaged two SM measurements (taken 1 m apart) integrated from the surface to the depth of 0.5 m could explain their better results. As regards to site C, the straightforward comparison of the GEM-300 measurement with SM measured at 0.3 and 0.6 m implicitly assumes that those specific layers mostly influence the EMI response and disregards the contribution of the upper SM. The higher correlation reported by Sherlock and McDonnell (2003) for point SM and EC_a at depth similar to those of sites A, B and D might be related to the absence of clay minerals in their study site. Popp et al. (2012) observed similar correlations for EC_a and SM measured up to 0.40 m in soils with a clay content up to 30%. A similarly low correlation value was reported by Robinson et al. (2012) for 0.15 m SM depth in an area containing clay and silty-clays.

As mentioned previously, although the signal variability of the GEM-300 was shown to be small, positional variations introduced additional variability in the instrumental response. In order to reduce the noise in the original point measurements, an algorithm for 2D smoothing was applied to the gridded data of SM and EC_a

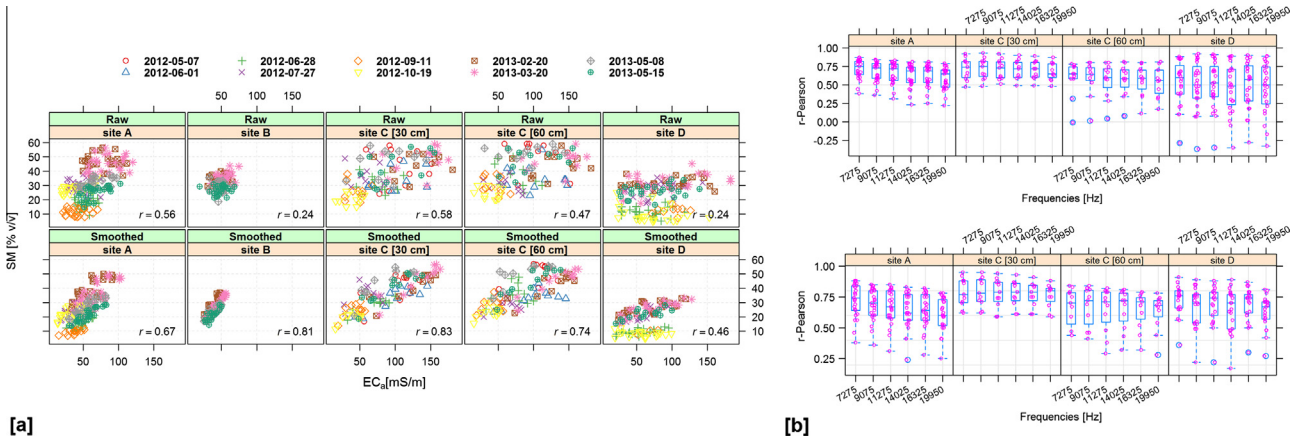

Fig. 5. (a) Correlation (r) between SM and EC_a (7275 Hz) in each site for raw (upper) and smoothed (lower) values. (b) Comparison of the distributions of the correlation (r) between point SM and EC_a for the six frequencies in each site. Both raw (upper) and smoothed (lower) data are showed.

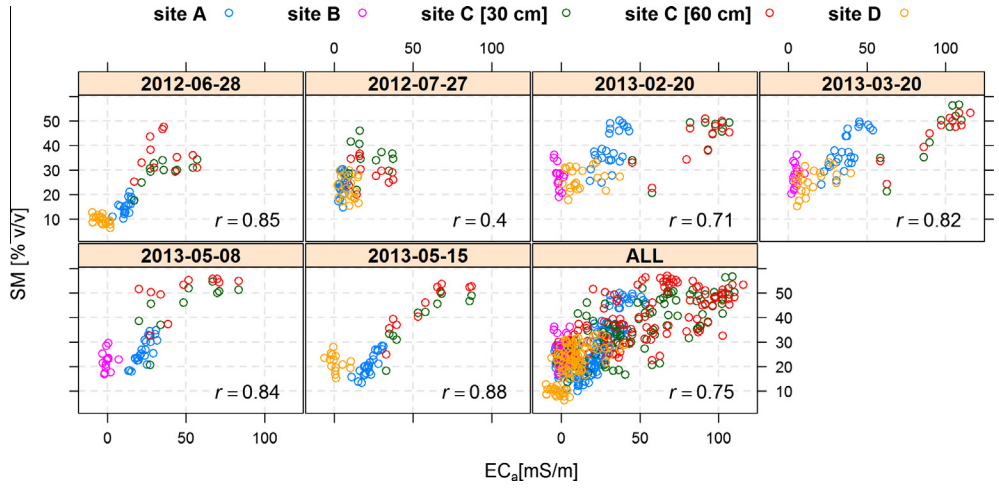

Fig. 6. Correlation (r) for each survey between SM and EC_a (7275 Hz) differences with respect to the drier date for each site.

and resulted in a clear raise of the correlation (Fig. 5). The relation between smoothed point EC_a and SM well agrees with results of other authors for similar depths (Hezarjaribi and Sourell, 2007; Robinson et al., 2008c, 2009). The SM variance explained by EC_a for site C (0.3 and 0.6 m) is comparable with the results of Hezarjaribi and Sourell (2007) and of Robinson et al. (2008c), while it is higher than that reported by Robinson et al. (2009). The effect of the spatial smoothing may be explained by considering that it smoothes out the variability induced on the EMI sensor by "disturbing factors", such as the occasional presence of iron objects, the position of the sensor (i.e. height and tilting) relatively to the ground and the presence of phone or power lines. Further, the smoothing removes part of the small-scale variability due to the heterogeneity of soil physical properties. Indeed, the relatively smaller TDR support volume (order of magnitude $\sim 10^3$ cm^3) can easily be affected by small-scale heterogeneity of the soil, such as the presence of air pocket close to stones or created by cracks in the soil. Therefore, given the point-scale nature of the TDR measurement, the spatial SM patterns thus delineated reflect small-scale variations that probably do not describe well the actual spatial patterns at a larger scale.

In order to understand how well EC_a measurements can describe SM distribution from the catchment perspective, the data set was split by survey dates. Considering that properties other than SM can influence soil EC_a (Friedman, 2005) a differencing approach proposed by Robinson et al. (2009, 2012) was applied. For a given site, EC_a differences were calculated respect to the driest dates, September for site A and October for all the other sites (Fig. 4a). Data collected during the first two surveys (May and June 2012) are not considered here since only site C was sampled. Excluding the survey of July, the SM variance explained by the rescaled EC_a temporal variations remained quite high ($R^2 < \sim 50\%$) (see Fig. 6). These results substantially agree with the intuition of Robinson et al. (2009, 2012) to use differences between EMI measurements in order to remove the contribution due to the solid matrix mineral and to isolate the effect of the SM dynamics on the EC_a variations. Future efforts will focus on the use of ΔEC_a obtained by time-lapse approach to feed physical electrical models (Friedman, 2005; Binley et al., 2015) for SM prediction.

4.4. Estimation of soil moisture from GEM-300

Based on the results of the previous section, the relationship between smoothed SM and EC_a measurements was developed by assuming a linear correlation (Table 4). In the following, site D will be neglected due to the previous discussions. As regards to site B, it will not be considered on its own due to the limited number of surveys available. However, data collected at site B will be used together with those of site A where data were collected at the same depth and with the same sampling scheme.

Table 4
slope, intercept, RMSE and coefficient of determination R^2 relating smoothed point SM to smoothed point ECa (freq. 7275 Hz). The number of points used is also reported (*N*).

	Slope	Intercept	RMSE (% cm^3/cm^3)	R^2	*N*
Site A	0.37	6.7	7.6	0.46	200
Site A + B	0.34	9.4	6.9	0.42	300
Site C (30 cm)	0.24	14.9	6.4	0.69	110
Site C (60 cm)	0.21	19.7	7.7	0.54	110

In this section, it is assumed that the smoothed values more adequately represent the actual SM pattern in the field at the hillslope spatial scale. A single linear relation was fitted for each site, named hereafter 'site model', considering all data collected during the surveys. The additional regression model calibrated grouping together site A and site B data will be referred as 'pooled model'.

Although the accuracies of the calibration equations were commensurate among sites, the measurements of EC_a captured a higher proportion of the spatio-temporal variance of SM at site C than at site A (Table 4). In addition to the already discussed issues related to the depths of investigation and SM variability, other factors play an important role with regard to the explained SM variance. Indeed, the degree of the correlation between SM and EC_a at the Fiumarella sites (Table 4) is higher in those zones of the catchment (western and central) where a lower amount of smectite has been described (Cavalcante et al., 2015) basically agreeing with other authors (Abdu et al., 2008).

The calibration parameters estimated on smoothed data were applied to 'raw' EC_a data to estimate SM. In order to assess the accordance between predicted and measured SM values in the temporal domain, areal averages and their respective confidence intervals (CI) at 95% probability were estimated. The temporal evolution of the predicted mean SM curves reproduced reasonably well those of the measured SM (Fig. 7). The 'site model' allowed recognizing the seasonal drying down, from May to October 2012, as well as the wetting after the fall/winter rainfall. Generally, the temporal evolution of SM was more accurately and precisely predicted at site C, with RMSE = 4.5% and 6.0% for SM at 0.3 and 0.6 m, respectively, than at site A (RMSE = 7.8%) where shallower SM was measured. The temporal variations of the measured SM at 0.3 m were only slightly better predicted than at 0.6 m. The predictions were generally less accurate in

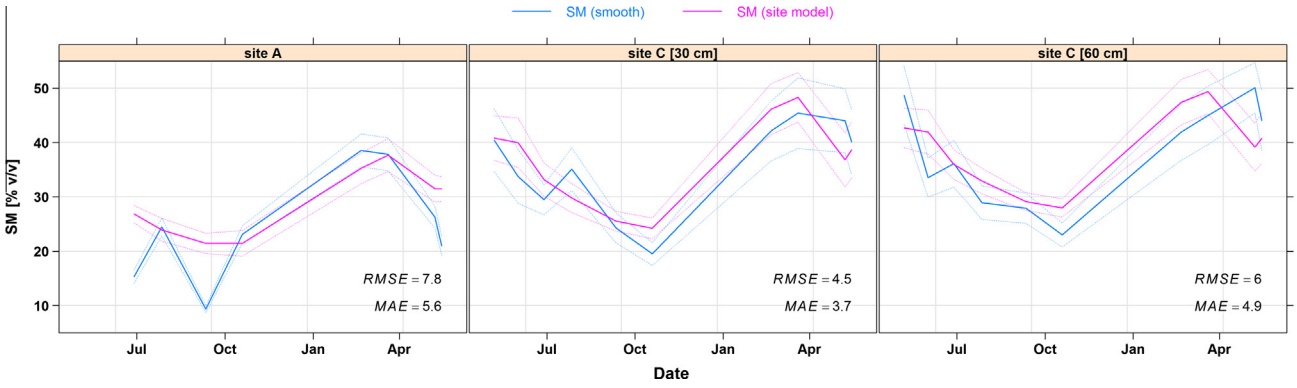

Fig. 7. Temporal trends of measured (smoothed) and predicted SM spatial means (solid lines) with their respective confidence intervals at 95% probability (dotted lines). The predictions showed are obtained using the EC_a from 7275 Hz frequency. Summary error statistics are also showed.

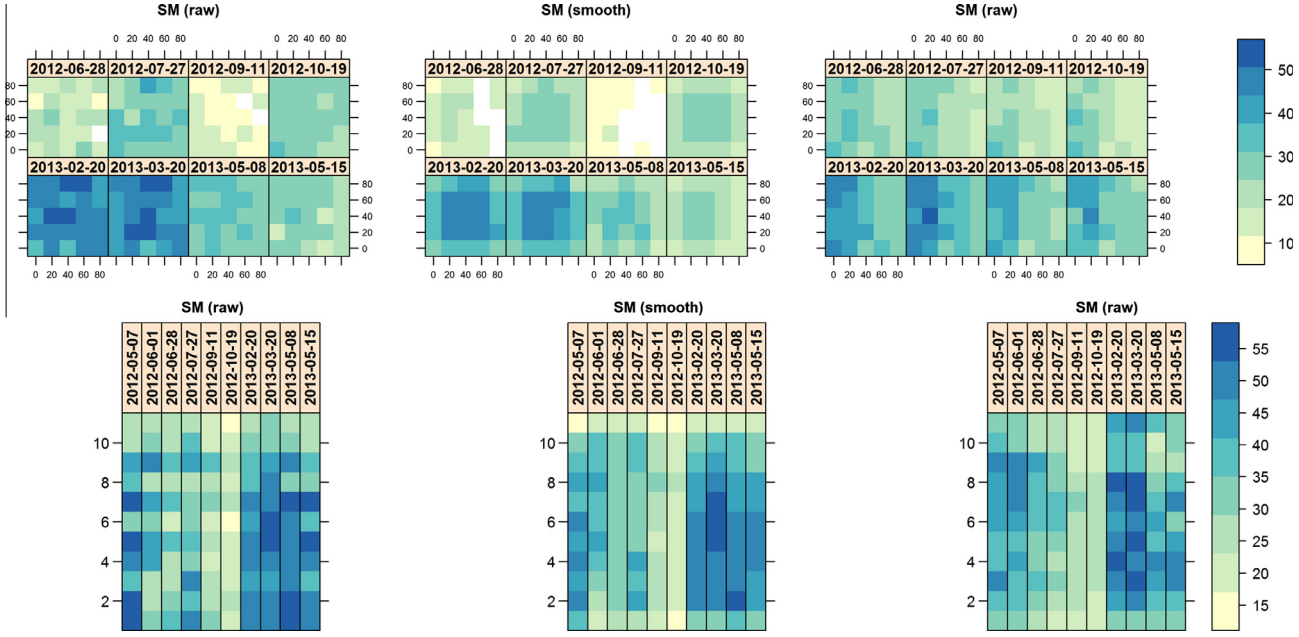

Fig. 8. SM comparison between measured (raw and smoothed) SM maps and predicted EMI-SM maps for site A-0.15 m (upper) and C-0.30 m (lower).

determining the dryer SM conditions, i.e. September for site A and October for site C. At site A, the overestimations of the measured SM spatial average was more severe. As regards to pooled model (Table 4), the SM spatial averages were estimated with a RMSE of 8.7% and 3.2% for site A and B, respectively.

The large overlap of the CI bands of measured and predicted SM, indicated that not only the tendency of SM in time can be inferred by EC_a data but that the predicted means were reasonably similar. Anyway some issues are worth to be considered. Binley et al. (2015) pointed out that the capability of having a mobile sensor to measure volume of soils not normally achievable with traditional SM sensors is an advantage often overlooked. They follow saying: *"[...] it does present challenges as we strive to assess these new techniques but are constrained by verification from "acceptable" measurement approaches based on a much smaller spatial scale [...]"*. Beyond debatable accuracies issues the possibility of acquire much more data on relatively larger sample soils, characterize larger and wooded areas is definitely an added value for frequency domain EMI sensor. This is especially true in the emerging spirit of mutual exchange of information between geophysics and hydrology.

Though the above analysis proved the possibility to follow the drying and wetting temporal trend of the SM areal average by means of the EMI predicted SM values, a further step would be to study how the predicted spatial fluctuations mimic those of the measured SM. By considering that the sampling strategy adopted was not designed to explicitly study spatial variability of SM, only a qualitative analysis is undertaken here. Fig. 8 shows a comparison between the SM maps obtained through the raw and smoothed TDR measurements and the 'site model' applied to EC_a data for site A and C (0.3 m). As expected, the temporal evolution of the maps still allows following the drying and wetting pattern at the investigated sites. Moreover, at site C the spatial pattern is quite well reproduced as dry and wet areas are recognizable in both TDR and GEM-300 maps.

5. Conclusions

The appropriateness of the multi-frequency sensor GEM-300 for the spatio-temporal retrieval of SM at the hillslope scale has been evaluated in four sites located in the small mountainous catchment of the "Fiumarella di Corleto" (32 km^2) in southern Italy.

The GEM-300 is one of the less employed sensors for hydrological applications. In order to test its suitability to resolve the spatio-temporal variations at our sites, the measurement precision of the sensor was firstly assessed. The inherent signal variability of the GEM-300 was shown to be a small fraction of the spatial and temporal EC_a variability at the Fiumarella catchment during tests on a fixed point. However, additional variability, which does not reflect physical changes in the soil property of interest, is introduced in the signal by positional variations of the sensor. These signal variations, which are practically unavoidable when an operator carries the sensor, were filtered out by using a simple moving average.

Six frequencies were chosen in the range between ~7 and 20 kHz for the GEM-300. Although systematic lower values of EC_a were measured at ~14 kHz, the EC_a values measured from the six frequencies were highly correlated both in time and space. However, in most cases the lower frequencies, i.e. 7 and 9 kHz, correlate slightly better than the higher, i.e. 20 kHz, with SM.

In order to assess in which conditions the GEM-300 sensor could be used for the retrieval of SM variations during a complete hydrological year, a number of sites with different soil-landscape attributes were surveyed. Raw SM and EC_a point data showed low correlations comparable with some published studies. This result should be attributed to the challenging conditions (complex terrain and forested coverage) in which SM and EC_a measurements were carried out and to the significant presence of high conductive minerals (2:1 clays) at one of the sites (site D) that masks the relationship between SM and EC_a. Indeed, the application of a spatial smoothing filter reduces the noises due to the GEM-300 sensor positioning (height and tilting) and the difference in the investigated soil volume of the two sensors (TDR and GEM-300). Based on the results of the correlation analysis, a linear relationship between EC_a and SM measurements was built with different degrees of explained variance (e.g., $R^2 \sim = 0.46–0.69$) and confidence (e.g. RMSE ~3.2–7.8), with best results obtained in the wooded areas. The linear relationship was used for mapping SM from EC_a measurements allowing us to visualize the spatial–temporal agreement between the two measurements.

Notwithstanding the accuracy of the SM values predicted on the base of the GEM-300 measurements at the investigated sites is not at a level usually considered desirable, the possibility to collect data quickly on relatively extended areas, with a significant reduction of time and effort, makes the EMI method appealing technique with some restrictions. Its reliability is limited at the point scale, but increases after smoothing making it a valuable tool for supporting hydrological studies at small-catchment scale and for the validation of coarse-scale satellite SM products. However, it was found that a number of disturbing factors could make the interpretation of the signal still challenging (see e.g., at site D). Therefore, additional information (spatial distribution of EC_w and clay; types of clay minerals and cross-correlation for SM and EC_a) is needed in order to better understand spatial issues related to the use of the EMI method for SM monitoring.

Acknowledgments

The authors wish to thank F. Cavalcante, G. Corrado, S. Margiotta and C. Belviso for their participation in discussion and for sharing unpublished results. This research was carried out within the framework of activities of the CINID under the research agreement with the Civil Protection of the Basilicata Region.

References

Abdu, H., Robinson, D.A., Seyfried, M., Jones, S.B., 2008. Geophysical imaging of watershed subsurface patterns and prediction of soil texture and water holding capacity. Water Resour. Res. 44 (4).

Akbar, M.A., Kenimer, A.L., Searcy, S.W., Torbert, H.A., 2005. Soil water estimation using electromagnetic induction. Transact. ASAE 48 (1), 129–135.

Binley, A., Hubbard, S.S., Huisman, J.A., Revil, A., Robinson, D.A., Singha, K., Slater, L.D., 2015. The emergence of hydrogeophysics for improved understanding of subsurface processes over multiple scales. Water Resour. Res. 51. http://dx.doi.org/10.1002/2015WR017016.

Brevik, E.C., Fenton, T.E., Lazari, A., 2006. Soil electrical conductivity as a function of soil water content and implications for soil mapping. Precision Agric. 7 (6), 393–404. http://dx.doi.org/10.1007/s11119-006-9021-x.

Brocca, L., Melone, F., Moramarco, T., Morbidelli, R., 2009. Soil moisture temporal stability over experimental areas in Central Italy. Geoderma 148 (3–4), 364–374. http://dx.doi.org/10.1016/j.geoderma.2008.11.004.

Brocca, L., Moramarco, T., Melone, F., Wagner, W., Hasenauer, S., Hahn, S., 2012b. Assimilation of surface- and root-zone ASCAT soil moisture products into rainfall-runoff modeling. IEEE Trans. Geosci. Remote Sens. 50 (7), 2542–2555. http://dx.doi.org/10.1109/TGRS.2011.2177468.

Brocca, L., Ponziani, F., Moramarco, T., Melone, F., Berni, N., Wagner, W., 2012a. Improving landslide forecasting using ASCAT-derived soil moisture data: a case study of the Torgiovannetto Landslide in central Italy. Remote Sens. 4 (5), 1232–1244, Retrieved from <http://www.mdpi.com/2072-4292/4/5/1232/pdf>.

Bronstert, A., Creutzfeldt, B., Graeff, T., Hajnsek, I., Heistermann, M., Itzerott, S., Jagdhuber, T., Kneis, D., Lück, E., Reusser, D., Zehe, E., 2012. Potentials and constraints of different types of soil moisture observations for flood simulations in headwater catchments. Nat. Hazards 60 (3), 879–914. http://dx.doi.org/10.1007/s11069-011-9874-9.

Buchanan, S., Triantafilis, J., 2009. Mapping water table depth using geophysical and environmental variables. Ground Water 47 (1), 80–96. http://dx.doi.org/10.1111/j.1745-6584.2008.00490.x.

Calamita, G., Brocca, L., Perrone, A., Piscitelli, S., Lapenna, V., Melone, F., Moramarco, T., 2012. Electrical resistivity and TDR methods for soil moisture estimation in central Italy test-sites. J. Hydrol. 454, 101–112.

Callegary, J.B., Ferré, T.P.A., Groom, R.W., 2007. Vertical spatial sensitivity and exploration depth of low-induction-number electromagnetic-induction instruments. Vadose Zone J. 6 (1), 158. http://dx.doi.org/10.2136/vzj2006.0120.

Callegary, J.B., Ferré, T.P.A., Groom, R.W., 2012. Three-dimensional sensitivity distribution and sample volume of low-induction-number electromagnetic-induction instruments. Soil Sci. Soc. Am. J. 76 (1). http://dx.doi.org/10.2136/sssaj2011.0003.

Carriero, D., Romano, N., Fiorentino, M., 2007. A simplified approach for determining hydrologic behaviour and depth of soils at basin scale. J. Agr. Eng. 2, 1–10.

Cavalcante, F., Prosser, G., Agosta, F., Belviso, C., Corrado, G., 2015. Post-depositional history of the Miocene Gorgoglione Formation (southern Apennines, Italy): inferences from mineralogical and structural analyses. Bulletin de la Société géologique de France 186 (4–5), 243–256. http://dx.doi.org/10.2113/gssgfbull.186.4-5.243.

Corwin, D.L., Lesch, S.M., 2005. Characterizing soil spatial variability with apparent soil electrical conductivity: I. Survey protocols. Comput. Electron. Agric. 46 (1), 103–133.

Corwin, D.L., Plant, R.E., 2005. Applications of apparent soil electrical conductivity in precision agriculture. Comput. Electron. Agric. 46 (1–3), 1–10. http://dx.doi.org/10.1016/j.compag.2004.10.004.

Dafflon, B., Hubbard, S.S., Ulrich, C., Peterson, J.E., 2013. Electrical conductivity imaging of active layer and permafrost in an arctic ecosystem, through advanced inversion of electromagnetic induction data. Vadose Zone J. 12 (4). http://dx.doi.org/10.2136/vzj2012.0161.

De Smedt, P., Saey, T., Lehouck, A., Stichelbaut, B., Meerschman, E., Islam, M.M., Van Meirvenne, M., 2013. Exploring the potential of multi-receiver EMI survey for geoarchaeological prospection: a 90ha dataset. Geoderma 199, 30–36. http://dx.doi.org/10.1016/j.geoderma.2012.07.019.

Doolittle, J.A., Brevik, E.C., 2014. The use of electromagnetic induction techniques in soils studies. Geoderma 223–225, 33–45. http://dx.doi.org/10.1016/j.geoderma.2014.01.027.

Doolittle, J., Petersen, M., Wheeler, T., 2001. Comparison of two electromagnetic induction tools in salinity appraisals. J. Soil Water Conserv. 56 (3), 257–262.

El-Qady, G., Metwaly, M., Khozaym, A., 2014. Tracing buried pipelines using multi frequency electromagnetic. NRIAG J. Astron. Geophys. 3 (1), 101–107. http://dx.doi.org/10.1016/j.nrjag.2014.06.002.

Evett, S.R., Heng, L.K., Moutonnet, P., Nguyen, M.L., 2008. Field Estimation of Soil Water Content: A Practical Guide to Methods, Instrumentation, and Sensor Technology. IAEA, Vienna.

Fiorentino, M., Carriero, D., Iacobellis, V., Manfreda, S., Portoghese, I., 2006. MEDCLUB – starting line and first activities. In: Sivapalan, M., Wagener, T., Uhlenbrook, S., Zehe, E., Lakshmi, V., Liang, X., Tachikawa, Y., Kumar, P. (Eds.), Predictions in Ungauged Basins: Promises and Progress. IAHS Publication 303, ISBN 1-901502-48-1.

Friedman, S.P., 2005. Soil properties influencing apparent electrical conductivity: a review. Comput. Electron. Agric. 46 (1), 45–70.

Hanson, B.R., Kaita, K., 1997. Response of electromagnetic conductivity meter to soil salinity and soil–water content. J. Irrigat. Drain. Eng. 123 (2), 141–143. http://dx.doi.org/10.1061/(ASCE)0733-9437(1997) 123:2(141).

Hedley, C.B., Roudier, P., Yule, I.J., Ekanayake, J., Bradbury, S., 2013. Soil water status and water table depth modelling using electromagnetic surveys for precision irrigation scheduling. Geoderma 199, 22–29.

Hezarjaribi, A., Sourell, H., 2007. Feasibility study of monitoring the total available water content using non-invasive electromagnetic induction-based and electrode-based soil electrical conductivity measurements. Irrigation Drain. 56 (1), 53–65. http://dx.doi.org/10.1002/ird.289.

Hossain, M.B., Lamb, D.W., Lockwood, P.V., Frazier, P., 2010. EM38 for volumetric soil water content estimation in the root-zone of deep Vertosol Soils. Comput. Electron. Agric. 74 (1), 100–109.

Huang, H., 2005. Depth of investigation for small broadband electromagnetic sensors. Geophysics 70 (6), G135–G142.

Huisman, J.A., Snepvangers, J.J.J.C., Bouten, W., Heuvelink, G.B.M., 2002. Mapping spatial variation of surface soil water content: comparison of ground-penetrating radar and time domain reflectometry. J. Hydrol. 269, 194–207. http://dx.doi.org/10.1016/S0022-1694(02)00239-1.

Huth, N.I., Poulton, P.L., 2007. An electromagnetic induction method for monitoring variation in soil moisture in agroforestry systems. Soil Res. 45 (1), 63–72.

Kachanoski, R.G., Wesenbeeck, I.J.V., Gregorich, E.G., 1988. Estimating spatial variations of soil water content using non contacting electromagnetic inductive methods. Can. J. Soil Sci. 68 (4), 715–722. http://dx.doi.org/10.4141/cjss88-069.

Kachanoski, R.G., Wesenbeeck, I.J.V., Jong, E.D., 1990. Field scale patterns of soil water storage from non-contacting measurements of bulk electrical conductivity. Can. J. Soil Sci. 70 (3), 537–542. http://dx.doi.org/10.4141/cjss90-056.

Khakural, B.R., Robert, P.C., Hugins, D.R., 1998. Use of non-contacting electromagnetic inductive method for estimating soil moisture across a landscape. Commun. Soil Sci. Plant Anal. 29 (11–14), 2055–2065.

Larson, K.M., Small, E.E., Gutmann, E.D., Bilich, A.L., Braun, J.J., Zavorotny, V.U., 2008. Use of GPS receivers as a soil moisture network for water cycle studies. Geophys. Res. Lett. 35 (24).

Ma, R., McBratney, A., Whelan, B., Minasny, B., Short, M., 2011. Comparing temperature correction models for soil electrical conductivity measurement. Precision Agric. 12 (1), 55–66.

Manfreda, S., Caylor, K., 2013. On the vulnerability of water limited ecosystems to climate change. Water 5 (2), 819–833.

Manfreda, S., Lacava, T., Onorati, B., Pergola, N., Leo, M.D., Margiotta, M.R., Tramutoli, V., 2011. On the use of AMSU-based products for the description of soil water content at basin scale. Hydrol. Earth Syst. Sci. 15 (9), 2839–2852.

Manfreda, S., Fiorentino, M., 2008. A stochastic approach for the description of the water balance dynamics in a river basin. Hydrol. Earth Syst. Sci. 12 (5), 1189–1200.

Manfreda, S., McCabe, M., Wood, E.F., Fiorentino, M., Rodríguez-Iturbe, I., 2007. Spatial patterns of soil moisture from distributed modeling. Adv. Water Resour. 30 (10), 2145–2150. http://dx.doi.org/10.1016/j.advwatres.2006.07.009.

McDonnell, J.J., Sivapalan, M., Vaché, K., Dunn, S., Grant, G., Haggerty, R., Hinz, C., Hooper, R., Kirchner, J., Roderick, M.L., Selker, J., Weiler, M., 2007. Moving beyond heterogeneity and process complexity: a new vision for watershed hydrology. Water Resour. Res. 43 (7), W07301. http://dx.doi.org/10.1029/2006WR005467.

Ochsner, T.E., Cosh, M.H., Cuenca, R.H., Dorigo, W.A., Draper, C.S., Hagimoto, Y., Kerr, Y.H., Njoku, E.G., Small, E.E., Zreda, M., 2013. State of the art in large-scale soil moisture monitoring. Soil Sci. Soc. Am. J. 77 (6), 1888–1919. http://dx.doi.org/10.2136/sssaj2013.03.0093.

Padhi, J., Misra, R.K., 2011. Sensitivity of EM38 in determining soil water distribution in an irrigated wheat field. Soil Tillage Res. 117, 93–102. http://dx.doi.org/10.1016/j.still.2011.09.003.

Penna, D., Tromp-van Meerveld, H.J., Gobbi, A., Borga, M., Dalla Fontana, G., 2011. The influence of soil moisture on threshold runoff generation processes in an alpine headwater catchment. Hydrol. Earth Syst. Sci. 15 (3), 689–702. http://dx.doi.org/10.5194/hess-15-689-2011.

Popp, S., Altdorff, D., Dietrich, P., 2012. Assessment of shallow subsurface characterization with non-invasive geophysical methods at the intermediate hill-slope scale. Hydrol. Earth Syst. Sci. Discuss. 9, 2511–2539.

Reedy, R.C., Scanlon, B.R., 2003. Soil water content monitoring using electromagnetic induction. J. Geotech. Geoenviron. Eng. 129 (11), 1028–1039.

Robinson, D.A., Abdu, H., Lebron, I., Jones, S.B., 2012. Imaging of hill-slope soil moisture wetting patterns in a semi-arid oak savanna catchment using time-lapse electromagnetic induction. J. Hydrol. 416–417, 39–49. http://dx.doi.org/10.1016/j.jhydrol.2011.11.034.

Robinson, D.A., Lebron, I., Kocar, B., Phan, K., Sampson, M., Crook, N., Fendorf, S., 2009. Time-lapse geophysical imaging of soil moisture dynamics in tropical deltaic soils: an aid to interpreting hydrological and Geochemical Processes. Water Resour. Res. 45 (4).

Robinson, D.A., Binley, A., Crook, N., Day-Lewis, F.D., Ferré, T.P.A., Grauch, V.J.S., Knight, R., Knoll, M., Lakshmi, V., Miller, R., Nyquist, J., Pellerin, L., Singha, K., Slater, L., 2008a. Advancing process-based watershed hydrological research using near-surface geophysics: a vision for, and review of, electrical and magnetic geophysical methods. Hydrol. Process. 22 (18), 3604–3635. http://dx.doi.org/10.1002/hyp.6963.

Robinson, D.A., Campbell, C.S., Hopmans, J.W., Hornbuckle, B.K., Jones, S.B., Knight, R., Ogden, F., Selker, J., Wendroth, O., 2008b. Soil moisture measurement for ecological and hydrological watershed-scale observatories: a review. Vadose Zone J. 7 (1), 358. http://dx.doi.org/10.2136/vzj2007.0143.

Robinson, D.A., Abdu, H., Jones, S.B., Seyfried, M., Lebron, I., Knight, R., 2008c. Eco-geophysical imaging of watershed-scale soil patterns links with plant community spatial patterns. Vadose Zone J. 7 (4), 1132–1138.

Romano, N., Palladino, M., 2002. Prediction of soil water retention using soil physical data and terrain attributes. J. Hydrol. 265 (1), 56–75.

Rubol, S., Manzoni, S., Bellin, A., Porporato, A., 2013. Modeling soil moisture and oxygen effects on soil biogeochemical cycles including dissimilatory nitrate reduction to ammonium (DNRA). Adv. Water Resour. 62 (Part A), 106–124. http://dx.doi.org/10.1016/j.advwatres.2013.09.016.

Saey, T., Simpson, D., Vermeersch, H., Cockx, L., Van Meirvenne, M., 2009. Comparing the EM38DD and DUALEM-21S sensors for Depth-to-Clay mapping. Soil Sci. Soc. Am. J. 73 (1), 7. http://dx.doi.org/10.2136/sssaj2008.0079.

Samouëlian, A., Cousin, I., Tabbagh, A., Bruand, A., Richard, G., 2005. Electrical resistivity survey in soil science: a review. Soil Tillage Res. 83 (2), 173–193.

Santini, A., Coppola, A., Romano, N., Terribile, F., 1999. Interpretation of the spatial variability of soil hydraulic properties using a land system analysis. In: Feyen, J., Wiyo, K. (Eds.), Modelling of Transport Processes in Soils at Various Scales in Time and Space. Wageningen Pers, Wageningen, The Netherlands, pp. 491–500.

Scanlon, B.R., Paine, J.G., Goldsmith, R.S., 1999. Evaluation of electromagnetic induction as a reconnaissance technique to characterize unsaturated flow in an arid setting. Groundwater 37 (2), 296–304.

Seneviratne, S.I., Corti, T., Davin, E.L., Hirschi, M., Jaeger, E.B., Lehner, I., Orlowsky, B., Teuling, A.J., 2010. Investigating soil moisture-climate interactions in a changing climate: a review. Earth Sci. Rev. 99 (3–4), 125–161. http://dx.doi.org/10.1016/j.earscirev.2010.02.004.

Sharma, P.V., 1997. Environmental and Engineering Geophysics. Cambridge University Press.

Sheets, K.R., Hendrickx, J.M., 1995. Noninvasive soil water content measurement using electromagnetic induction. Water Resour. Res. 31 (10), 2401–2409.

Sherlock, M.D., McDonnell, J.J., 2003. A new tool for hillslope hydrologists: spatially distributed groundwater level and soil water content measured using electromagnetic induction. Hydrol. Process. 17 (10), 1965–1977. http://dx.doi.org/10.1002/hyp.1221.

Sivapalan, M., 2003. Process complexity at hillslope scale, process simplicity at the watershed scale: is there a connection? Hydrol. Process. 17 (5), 1037–1041. http://dx.doi.org/10.1002/hyp.5109.

Soil Moisture equipment Corp., 1996. Trase, Operating Instructions (Version 2000). Soil Moisture Equipment Corp., Santa Barbara, California.

Spies, B.R., 1989. Depth of investigation in electromagnetic sounding methods. Geophysics 57 (4), 872–888.

Stanley, J.N., Lamb, D.W., Irvine, S.E., Schneider, D.A., 2014. Effect of aluminum neutron probe access tubes on the apparent electrical conductivity recorded by an electromagnetic soil survey sensor. IEEE Geosci. Remote Sens. Lett. 11 (1), 333–336.

Sudduth, K.A., Drummond, S.T., Kitchen, N.R., 2001. Accuracy issues in electromagnetic induction sensing of soil electrical conductivity for precision agriculture. Comput. Electron. Agric. 31 (3), 239–264. http://dx.doi.org/10.1016/S0168-1699(00)00185-X.

Topp, G.C., Davis, J.L., Annan, A.P., 1980. Electromagnetic determination of soil water content: measurements in coaxial transmission lines. Water Resour. Res. 16 (3), 574–582.

Tromp-van Meerveld, H.J., McDonnell, J.J., 2009. Assessment of multi-frequency electromagnetic induction for determining soil moisture patterns at the hillslope scale. J. Hydrol. 368 (1), 56–67.

Vereecken, H., Huisman, J.A., Pachepsky, Y., Montzka, C., van der Kruk, J., Bogena, H., Weihermüller, L., Herbst, M., Martinez, G., Vanderborght, J., 2014. On the spatio-temporal dynamics of soil moisture at the field scale. J. Hydrol. 516, 76–96. http://dx.doi.org/10.1016/j.jhydrol.2013.11.061.

Won, I.J., Keiswetter, D., Fields, G., Sutton, L., 1996. GEM-2: a new multifrequency electromagnetic sensor. J. Environ. Eng. Geophys. 1 (2), 129–137.

Zreda, M., Shuttleworth, W.J., Zeng, X., Zweck, C., Desilets, D., Franz, T., Rosolem, R., Ferre, T.P.A., 2012. COSMOS: The COsmic-ray soil moisture observing system. Hydrol. Earth Syst. Sci. Discuss. 9 (4), 4505–4551. http://dx.doi.org/10.5194/hessd-9-4505-2012.